
Pharmolix-FM: An All-Atom Multi-Modal Foundation Model for Molecular Modeling and Generation

Yizhen Luo^{1,2,†,‡}, Jiashuo Wang^{1,2,†}, Siqi Fan^{1,2}, Zaiqing Nie^{1,2,*}

¹Pharmolix-FM Inc.

²Institute for AI Industry Research (AIR), Tsinghua University

{yz-luo22, wang-js21}@mails.tsinghua.edu.cn

{fansiqi, zaiqing}@air.tsinghua.edu.cn

Abstract

Atomic interactions lie at the heart of molecular structures and functions, serving as the foundation for a wide range of molecular interaction tasks. To establish a unified framework for modeling diverse molecular systems, we propose Pharmolix-FM, a generative model that operates at the all-atom level, enabling consistent representation and interaction modeling across different biomolecules. Pharmolix-FM integrates multiple state-of-the-art generative modeling approaches and allows for unified evaluation across multiple tasks without the need for fine-tuning. Through a systematic comparison of different generative algorithms within this framework, we provide a comprehensive analysis of their effectiveness in molecular interaction tasks. Experimental results demonstrate that Pharmolix-FM achieves superior performance across various tasks, highlighting its potential for advancing molecular interaction modeling. Our code will be publicly available at <https://github.com/PharMolix/OpenBioMed>.

1 Introduction

Atoms, amino acids, and nucleic acids are fundamental components of life, their interactions determine key biological processes such as protein structure, enzymatic catalysis of proteins and cell signaling. Understanding these interactions is critical to unraveling the molecular mechanisms of cellular functions. The development in the field of deep learning (DL) presents an approach distinct from traditional methods[1]. The field of DL has developed an approach distinct from traditional methods by treating the tasks of molecular interactions as regression or generation tasks. Numerous studies have indicated that, compared with traditional methods, DL methods demonstrate improvements in both performance and inference efficiency across various molecular interaction tasks[2–4].

In recent years, all-atom modeling has gained increasing attention in fields such as molecular simulation and drug discovery. Compared to coarse-grained representations, all-atom modeling enables more precise capture of intermolecular interactions, such as van der Waals forces and hydrogen bonding, thereby enhancing the accuracy of molecular behavior modeling. For example, in docking tasks, early machine learning methods typically represented proteins at the residue level[5, 6], whereas all-atom approaches can preserve crucial geometric details, such as side-chain conformations, making them more suitable for high-precision modeling. Recently, models such as AlphaFold3 [7] and PocketXMol [8] have adopted all-atom modeling strategies, achieving significant progress in biomolecular structure prediction and molecular docking tasks. These works demonstrate that all-

[†]Equal Contribution.

[‡]Work done during internship in Pharmolix-FM Inc.

^{*}Corresponding author

atom representations not only improve model generalizability but also enhance adaptability across different molecular types and tasks.

Despite its advantages across multiple tasks, all-atom modeling still faces significant challenges in the development of foundation models (FMs) with strong generalization capabilities. First, early molecular modeling approaches were often optimized for specific tasks, and there has been limited effort toward establishing a unified representation that can seamlessly transfer across different molecular types and interaction tasks [9, 10]. Second, while all-atom representations provide fine-grained interaction details, they also introduce substantial computational costs, making it challenging to train FMs on large-scale datasets. Additionally, most existing all-atom modeling approaches rely on specific generative paradigms to capture molecular interactions, yet there has been limited systematic comparison across different generative methods. This lack of comparative studies constrains our understanding of the optimal strategies for all-atom modeling.

To address these challenges, we propose Pharmolix-FM, which leverages local protein pocket information within a 10 Å range instead of the entire protein to precisely characterize binding sites and their interactions. By focusing on the key interaction regions, our approach reduces computational complexity while preserving critical all-atom interaction details. Furthermore, we implement both Diffusion based[11] and Bayesian Flow Networks (BFN) based[12] generative paradigms, allowing for a systematic comparison of these two approaches within a unified framework.

To validate our approach, we conducted comprehensive evaluations on the PoseBusters benchmark and assessed binding affinity and drug-like properties. Our results demonstrate that both Diffusion based and BFN based models achieve comparable or superior performance to PocketXMol. Specifically, our Diffusion model outperforms PocketXMol in self-ranking accuracy (81.07% vs. 78.97%), while both generative paradigms maintain competitive performance in oracle-ranking ,molecular binding affinity and drug-like properties. These findings highlight the potential of diverse generative paradigms in advancing all-atom molecular modeling.

2 Methodology

2.1 Preliminaries

Notations. Let $\mathcal{A}_{\text{mol}} = [a_i^{\text{mol}}]$ represent the atom types for a given molecule, where a_i^{mol} denotes the atom type of the i -th atom. Similarly, $\mathcal{X}_{\text{mol}} = [x_i^{\text{mol}}]$ represents the atomic coordinates for the molecule and $\mathcal{B}_{\text{mol}} = [b_i^{\text{mol}}]$ as the bond types for the molecule. Similarly, let $\mathcal{A}_{\text{poc}} = [a_i^{\text{poc}}]$, $\mathcal{X}_{\text{poc}} = [x_i^{\text{poc}}]$, and $\mathcal{B}_{\text{poc}} = [b_{ij}^{\text{poc}}]$ represent the atom types, atomic coordinates, and bond types respectively for the protein pocket. Moreover, We define \mathcal{P} as a set of indicators specifying whether certain molecular properties are fixed during training. Specifically, \mathcal{P}_A includes indicators for whether atom types and atomic coordinates are fixed, as well as whether the atoms belong to peptides. Similarly, \mathcal{P}_B includes indicators for whether bond types are fixed and whether interatomic distances are fixed. These indicators are designed to specify which molecular properties remain unchanged in different tasks where partial ground truth data needs to be provided.

2.2 Model Formulation

2.2.1 Model Architecture

Our study adopts a molecular encoding framework based on PocketXMol, designed to update atomic features, bond features, and atomic coordinates. For the encoder of the all-atom representation of the protein pocket, we construct a pocket atom graph \mathcal{G}_{poc} using a k -nearest neighbor (k-NN) graph (where $k = 32$). We iteratively update node representations through a custom block Ψ_{poc} (referred to as PocketBlock), which is constructed by Linear and MLP layers:

$$V_{\text{poc}} = \Psi_{\text{poc}}(\mathcal{G}_{\text{poc}}, \mathcal{A}_{\text{mol}}, \mathcal{X}_{\text{mol}}) \quad (1)$$

For the encoder of the molecule, we construct a complete graph \mathcal{G}_{mol} using the molecular atoms and a k-NN dynamic bipartite graph $\mathcal{G}_{\text{mol-poc}}$ between the molecule atoms and the pocket atoms (where $k = 32$). Then, to incorporate these property - fixed indicators, we concatenate \mathcal{P}_A and \mathcal{P}_B with the corresponding molecular property matrices \mathcal{A}_{mol} and \mathcal{B}_{mol} respectively:

$$V_{\text{mol}} = \text{concat}(\text{Linear}(\mathcal{A}_{\text{mol}}), \mathcal{P}_A)) \quad (2)$$

$$E_{\text{mol}} = \text{concat}(\text{Linear}(\mathcal{B}_{\text{mol}}), \mathcal{P}_B)) \quad (3)$$

After obtaining V_{mol} (node features) and E_{mol} (edge features), we use Ψ_{dist} (DistanceBlock) to calculate the features, relative vectors, and distances of edges within graph:

$$E_{\text{mol-poc}}, R_{\text{mol-poc}}, D_{\text{mol-poc}} = \Psi_{\text{dist}}(\mathcal{G}_{\text{mol}}, \{X_{\text{mol}}, X_{\text{poc}}\}) \quad (4)$$

Finally, we fed features and graphs into a framework consisting of three dedicated blocks: Ψ_{node} (NodeBlock), Ψ_{edge} (EdgeBlock), and Ψ_{pos} (PosBlock). These blocks are designed to iteratively update the molecular node and edge features, as well as predict the coordinate changes of the atoms:

$$V_{\text{mol}} = \Psi_{\text{node}}(V_{\text{mol}}, E_{\text{mol}}, \mathcal{G}_{\text{mol}}, V_{\text{poc}}, E_{\text{mol-poc}}, \mathcal{G}_{\text{mol-poc}}) \quad (5)$$

$$E_{\text{mol}} = \Psi_{\text{edge}}(E_{\text{mol}}, V_{\text{mol}}) \quad (6)$$

$$X_{\text{mol}} = X_{\text{mol}} + \Psi_{\text{pos}}(V_{\text{mol}}, E_{\text{mol-poc}}, R_{\text{mol-poc}}, D_{\text{mol-poc}}, V_{\text{poc}}) \quad (7)$$

Finally, a simple decoder layer is designed to take V_{mol} , E_{mol} and X_{mol} as inputs, predicting the probabilities of atom types and edge types, along with atomic coordinates and model confidence scores.

2.2.2 Training Objective

The loss function is designed to incorporate six terms, formulated as:

$$L = 1.5L_{\text{atom}} + 2.5L_{\text{coor}} + 1.5L_{\text{bond}} + L_{\text{cf}} \quad (8)$$

Specifically, L_{atom} , L_{coor} , and L_{bond} are the loss for predicted atom types, atomic coordinates and bond types. Meanwhile, L_{cf} is incorporated to ensure the reliability of confidence scores in model predictions.

2.3 Diffusion and BFN Paradigms

Diffusion based model. For Diffusion Models, we adopt the Denoising Diffusion Probabilistic Models (DDPM) framework. The noise addition process is defined as:

$$q(x_t|x_0) = \mathcal{N}(x_t | \sqrt{\bar{\alpha}_t}x_0, (1 - \bar{\alpha}_t)I) \quad (9)$$

Here, x_0 represents the original molecule structure, x_t is the corrupted version at time step t , and $\bar{\alpha}_t$ is a variance schedule that gradually increases the noise level.

During the sampling process, we use the following reverse transition:

$$q(x_{t-1}|x_t, x_0) = \mathcal{N}(x_{t-1} | \tilde{\mu}_t(x_t, x_0), \tilde{\beta}_t I) \quad (10)$$

where $\tilde{\mu}_t(x_t, x_0)$ is the mean of the reverse distribution, given by:

$$\tilde{\mu}_t(x_t, x_0) := \frac{\sqrt{\bar{\alpha}_{t-1}}\beta_t}{1 - \bar{\alpha}_t}x_0 + \frac{\sqrt{\alpha_t}(1 - \bar{\alpha}_{t-1})}{1 - \bar{\alpha}_t}x_t \quad (11)$$

and $\tilde{\beta}_t$ is the variance schedule for the reverse process.

Bayesian Flow Networks based model. For Bayesian Flow Networks (BFN), we separately model the noise perturbation for continuous and discrete variables. For continuous variables, the noise perturbation is defined as:

$$p_F(\theta|x; t) = \mathcal{N}(\mu | \gamma(t)x, \gamma(t)(1 - \gamma(t))I) \quad (12)$$

where x represents the ground truth structure, t denotes the noise level, and $\gamma(t)$ is a time-dependent function controlling the magnitude of noise added. For discrete variables, we introduce the following noise formulation:

$$p_F(\theta|x; t) = \mathbb{E}_{N(y|\beta(t)(Kx_e - 1), \beta(t)K)} \delta(\theta - \text{softmax}(y)) \quad (13)$$

where K is a scaling factor, x_e represents the encoded categorical input, and $\beta(t)$ is a time-dependent function that governs the variance of the noise applied to discrete variables.

The output distribution is modeled as:

$$\hat{x}(\theta, t) = \frac{\mu}{\gamma(t)} - \frac{1 - \gamma(t)}{\gamma(t)}\hat{\epsilon}(\theta, t) \quad (14)$$

where $\hat{\epsilon}(\theta, t)$ is the predicted noise at noise level t .

3 Experiments

3.1 Settings

3.1.1 Dataset Construction

We adopt the same training dataset and preprocessing pipeline as PocketXMol, which includes three categories of molecular data: (1) protein-small molecule complexes from PDBBind[13], Binding MOAD[14], and CrossDocked2020[15]; (2) protein-peptide complexes from PepBDB[16] and AlphaFoldDB[17]; and (3) small molecules from GEOM[18], CREMP[19], and Uni-Mol[20]. The dataset filtering and splitting follow the methodology in PocketXMol[8], ensuring consistency in data quality and avoiding information leakage. The validation set is extracted from the same datasets, with 100 samples from PDBBind, 100 from Binding MOAD, 100 from CrossDocked2020, 70 from PepBDB, 100 from AlphaFoldDB, 500 from GEOM-Drug, 500 from GEOM-QM9, 500 from CREMP, and 500 from Uni-Mol.

3.1.2 Evaluation

To evaluate our model across different molecular interaction tasks, we conducted experiments on two benchmark tasks:

Small Molecule Docking. We evaluated Pharmolix-FM on the PoseBusters benchmark, which consists of 428 protein-ligand complexes. To assess docking accuracy, we employed Root-Mean-Square Deviation (RMSD) as the evaluation metric. Specifically, we computed the atomic RMSD between the predicted and ground-truth molecular poses and measured the proportion of cases where $\text{RMSD} < 2\text{\AA}$ across the 428 protein-ligand complexes. Pharmolix-FM generated multiple poses per pocket and selected the top-ranked one using both self-ranking and a tuned ranking predictor.

Structure-Based Drug Design (SBDD). We evaluated Pharmolix-FM’s molecule generation performance using a test set derived from the CrossDocked dataset. Following standard preprocessing, we filtered out protein-ligand pairs with binding pose RMSD $> 1\text{\AA}$, resulting in a refined subset of 184,057 data points. We then applied MMseqs2[21] clustering at 30% sequence identity and randomly selected 100 protein pockets from distinct clusters for evaluation. For each pocket, we generated 100 molecules and assessed their quality using multiple metrics: QED (Quantitative Estimation of Drug-likeness) for drug-likeness, SA (Synthetic Accessibility) for synthetic feasibility, and AutoDock Vina to evaluate binding effectiveness by comparing binding affinities (Vina scores) with test set molecules. We compared Pharmolix-FM against existing methods, including the VAE-based liGAN, autoregressive models like 3DSBDD and Pocket2Mol, and Diffusion based methods such as TargetDiff and DecompDiff.

3.2 Performance on the Docking Task

Method	RMSD % below 2.0\text{\AA}	
	self-ranking	oracle-ranking
PocketXMol	78.97	94.16
BFN	78.27	93.45
Diffusion	81.07	94.16

Table 1: Comparison of RMSD % below 2.0\text{\AA} for different methods with the number of sampling set to 50.

Table 1 shows the evaluation results of Pharmolix-FM on the PoseBusters benchmark, with PocketXMol used as a comparison. In terms of self-ranking, the Diffusion based model outperformed PocketXMol, achieving an accuracy of 81.07% compared to PocketXMol’s 78.97%. Additionally, our BFN model also demonstrated a commendable performance, attaining an accuracy of 78.27%. In the oracle-ranking scenario, Pharmolix-FM’s Diffusion based model achieved 94.16%, which was identical to PocketXMol’s performance. These results demonstrate that different generative methods,

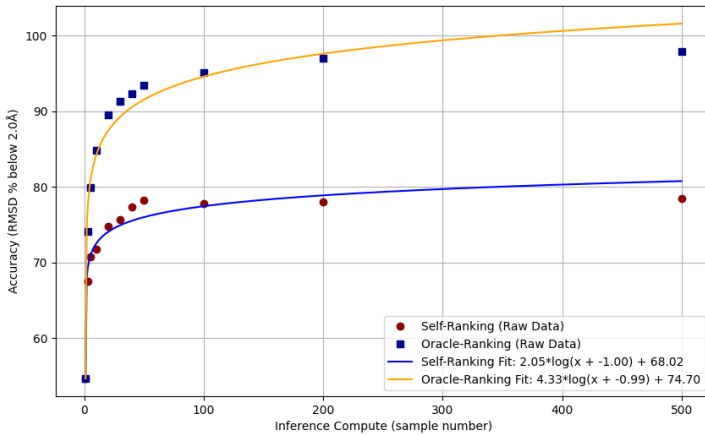


Figure 1: Inference Scaling Law.

including diffusion and BFN, can achieve comparable or even superior performance to PocketXMol. This highlights the effectiveness of alternative modeling approaches in capturing the interactions between proteins and ligands.

3.3 Performance on the SBDD Task

Method	Binding Affinity			Drug-like Property	
	vina_score↓ (Avg./Med.)	vina_min↓ (Avg./Med.)	vina_dock↓ (Avg./Med.)	QED↑ (Avg.)	SA↑ (Avg.)
Pocket2Mol	-5.14/-4.70	-6.42/-5.82	-7.15/6.79	0.57	0.76
TargetDiff	-5.47/-6.30	-6.64/-6.83	-7.80/-7.91	0.48	0.58
DecompDiff	-5.67/-6.04	-7.04/-7.09	-8.39/-8.43	0.45	0.61
MolCRAFT	-6.61/-8.14	-8.14/-8.42	-9.25/-9.20	0.46	0.62
PocketXMol	-6.06/-6.33	-7.16/-7.02	-8.07/-8.01	0.52	0.77
BFN	-6.38/-6.45	-6.97/-6.89	-7.68/-7.64	0.48	0.64
Diffusion	-6.18/-6.44	-7.19/-7.04	-7.88/-7.85	0.50	0.73

Table 2: Comparison of different methods on binding affinity and drug-like properties.

As presented in Table 2, both Diffusion and BFN, which are implemented by Pharmolix-FM, achieve a good balance between binding affinity and drug-like properties. Compared to the baseline method PocketXMol, they demonstrate better performance in vina_score (Diffusion: -6.18, BFN: -6.38 vs. PocketXMol: -6.06) and vina_min (Diffusion: -7.19, BFN: -6.97 vs. PocketXMol: -7.16), indicating that they generate molecules with stronger binding affinity. Meanwhile, their SA (synthetic accessibility) remains close to the baseline, ensuring reasonable synthesizability. In contrast, methods such as Pocket2Mol, TargetDiff, and DecompDiff generally perform worse in Binding Affinity and Drug-like Property. These results show that Diffusion and BFN perform well in both binding affinity and drug-like properties, demonstrating their potential in molecular generation.

3.4 Further Analysis

Inference Scaling Law We observe a clear scaling law behavior with respect to inference compute, where the computational cost is primarily determined by the number of samples. The accuracy of both self-ranking and oracle-ranking methods exhibits a logarithmic relationship with inference compute,

which can be empirically modeled as:

$$\text{Accuracy} = A \cdot \log(x + B) + C \quad (15)$$

where x represents the sample number, and A , B , C are constants. As shown in Figure 1, the accuracy improves significantly with increased inference compute (i.e., higher sample numbers), but the rate of improvement gradually diminishes, eventually approaching a plateau. This behavior aligns with the logarithmic scaling law, indicating that while increasing inference compute initially leads to substantial gains in accuracy, the marginal benefits decrease as compute grows larger.

4 Conclusion

In this work, we explored the effectiveness of all-atom molecular modeling using Diffusion based and BFN based generative paradigms within a unified framework. By leveraging local pocket information instead of full protein structures, our approach accurately captures key interaction features while maintaining computational efficiency. Experimental results on the PoseBusters benchmark demonstrate that both generative methods achieve comparable or superior performance to PocketXMol in molecular pose prediction and binding affinity evaluation. These findings highlight the potential of diverse generative strategies in advancing molecular modeling and pave the way for future research on efficient and generalizable foundation models for molecular interactions.

References

- [1] Michael M. Bronstein, Joan Bruna, Taco Cohen, and Petar Veličković. Geometric deep learning: Grids, groups, graphs, geodesics, and gauges. *ArXiv*, 2021.
- [2] Hannes Stärk, Octavian Ganea, Lagnajit Pattanaik, Regina Barzilay, and Tommi S. Jaakkola. Equibind: Geometric deep learning for drug binding structure prediction. In *ICML*, 2022.
- [3] Xingang Peng, Shitong Luo, Jiaqi Guan, Qi Xie, Jian Peng, and Jianzhu Ma. Pocket2mol: Efficient molecular sampling based on 3d protein pockets. In *ICML*, 2022.
- [4] Shitong Luo, Jiaqi Guan, Jianzhu Ma, and Jian Peng. A 3d generative model for structure-based drug design. In *NeurIPS*, 2021.
- [5] Gabriele Corso, Hannes Stärk, Bowen Jing, Regina Barzilay, and Tommi S. Jaakkola. Diffdock: Diffusion steps, twists, and turns for molecular docking. In *ICLR*, 2023.
- [6] Wei Lu, Jixian Zhang, Weifeng Huang, Ziqiao Zhang, Xiangyu Jia, Zhenyu Wang, Leilei Shi, Chengtao Li, Peter G. Wolynes, and Shuangjia Zheng. Dynamicbind: Predicting ligand-specific protein-ligand complex structure with a deep equivariant generative model. *Nature Communications*, 15(1):1071, February 2024.
- [7] Josh Abramson, Jonas Adler, Jack Dunger, et al. Accurate structure prediction of biomolecular interactions with AlphaFold 3. *Nature*, 630:493–500, 2024.
- [8] Xingang Peng, Ruihan Guo, Yan Xu, Jiaqi Guan, Yinjun Jia, Yanwen Huang, Muhan Zhang, Jian Peng, Jiayu Sun, Chuanhui Han, Zihua Wang, and Jianzhu Ma. Decipher fundamental atomic interactions to unify generative molecular docking and design. *bioRxiv*, 2024.
- [9] Shitong Luo, Chence Shi, Minkai Xu, and Jian Tang. Predicting molecular conformation via dynamic graph score matching. In *NeurIPS*, 2021.
- [10] Jiaxian Yan, ZAXI ZHANG, Jintao Zhu, Kai Zhang, Jianfeng Pei, and Qi Liu. Deltadock: A unified framework for accurate, efficient, and physically reliable molecular docking. In *NeurIPS*, 2024.
- [11] Jonathan Ho, Ajay Jain, and Pieter Abbeel. Denoising diffusion probabilistic models. In H. Larochelle, M. Ranzato, R. Hadsell, M.F. Balcan, and H. Lin, editors, *NeurIPS*, volume 33, pages 6840–6851. Curran Associates, Inc., 2020.
- [12] Alex Graves, Rupesh Kumar Srivastava, Timothy Atkinson, and Faustino Gomez. Bayesian flow networks. *arXiv preprint arXiv:2308.07037*, 2023.

- [13] Zhihai Liu, Yan Li, Li Han, Jie Li, Jie Liu, Zhixiong Zhao, Wei Nie, Yuchen Liu, and Renxiao Wang. Pdb-wide collection of binding data: current status of the pdbind database. *Bioinformatics*, 31(3):405–412, 10 2014.
- [14] M. L. Benson, R. D. Smith, N. A. Khazanov, B. Dimcheff, J. Beaver, P. Dresslar, J. Neroth, and H. A. Carlson. Binding moad, a high-quality protein-ligand database. *Nucleic Acids Research*, 36(Database issue):D674 – D678, Jan 2008.
- [15] P. G. Francoeur, T. Masuda, J. Sunseri, A. Jia, R. B. Iovanisci, I. Snyder, and D. R. Koes. Three-dimensional convolutional neural networks and a cross-docked data set for structure-based drug design. *Journal of Chemical Information and Modeling*, 60(9):4200–4215, Sep 2020.
- [16] Z. Wen, J. He, H. Tao, and S. Y. Huang. Pepbdb: a comprehensive structural database of biological peptide - protein interactions. *Bioinformatics*, 35(1):175 – 177, Jan 2019.
- [17] M. Varadi, D. Bertoni, P. Magana, U. Paramval, I. Pidruchna, M. Radhakrishnan, M. Tsenkov, S. Nair, M. Mirdita, J. Yeo, O. Kovalevskiy, K. Tunyasuvunakool, A. Laydon, A. Žídek, H. Tomlinson, D. Hariharan, J. Abrahamsen, T. Green, J. Jumper, E. Birney, M. Steinegger, D. Hassabis, and S. Velankar. Alphafold protein structure database in 2024: providing structure coverage for over 214 million protein sequences. *Nucleic Acids Research*, 52(D1):D368 – D375, Jan 2024.
- [18] Simon Axelrod and Rafael Gómez-Bombarelli. Geom, energy-annotated molecular conformations for property prediction and molecular generation. *Scientific Data*, 9(1):185, 04 2022.
- [19] Colin A. Grambow, Hayley Weir, Christian N. Cunningham, Tommaso Biancalani, and Kangway V. Chuang. Cremp: Conformer-rotamer ensembles of macrocyclic peptides for machine learning. *Scientific Data*, 11(1), August 2024.
- [20] Gengmo Zhou, Zhifeng Gao, Qiankun Ding, Hang Zheng, Hongteng Xu, Zhewei Wei, Linfeng Zhang, and Guolin Ke. Uni-mol: A universal 3d molecular representation learning framework. In *The Eleventh International Conference on Learning Representations*, 2023.
- [21] Milot Mirdita, Martin Steinegger, and Johannes Söding. Mmseqs2 desktop and local web server app for fast, interactive sequence searches. *Bioinformatics*, 35(16):2856–2858, 01 2019.